Journal of Crystal Growth 548 (2020) 125828

Contents lists available at ScienceDirect

Journal of Crystal Growth

journal homepage: www.elsevier.com/locate/jcrysgro

Optimization of the melt/crystal interface shape and oxygen concentration during the Czochralski silicon crystal growth process using an artificial neural network and a genetic algorithm

Xiaofang Qi[a,b], Wencheng Ma[a,*], Yifan Dang[c], Wenjia Su[a], Lijun Liu[c,*]

[a] School of Energy and Power Engineering, Institute for Energy Research, Jiangsu University, Zhenjiang, Jiangsu 212013, China
[b] Jiangsu Huantai Group Co., Ltd., Yangzhong, Jiangsu 212200, China
[c] School of Energy and Power Engineering, Xi'an Jiaotong University, Xi'an, Shaanxi 710049, China

ARTICLE INFO

Communicated by Chung wen Lan

Keywords:
A2. Czochralski silicon
A1. Melt/crystal interface shape
Oxygen concentration
A1. Artificial neural network
A1. Genetic algorithm

ABSTRACT

The melt/crystal interface shape and oxygen concentration during the Czochralski silicon crystal growth process significantly influence the crystal quality. In this paper, an optimization system with the combination of an artificial neural network and a genetic algorithm is proposed to optimize the growth parameters during the growth process. Flattening the melt/crystal interface and reducing the oxygen concentration along the interface were chosen as the optimization targets. Two important growth parameters, the crystal rotation rate and crucible rotation rate, were chosen as optimization variables. First, a global heat and mass transfer model was developed to simulate the crystal growth process and then tested with experimental data. The verified heat and mass transfer model was then used to train an artificial neural network with the aim of rapidly assessing the complex nonlinear dependence of the interface shape and oxygen concentration on the growth parameters. The trained neural network combined with a genetic algorithm was then used to obtain the optimal growth parameters. Both deflection of the melt/crystal interface and the oxygen concentration along the interface decreased after optimization. Finally, the optimal growth parameters were checked in the heat and mass transfer model to evaluate the performance of the optimization system. The proposed method will also be useful for optimization of other crystal growth processes.

1. Introduction

The Czochralski (CZ) growth method is the main method for production of large diameter and high quality monocrystalline silicon for the photovoltaic industry. With the rapid development of the photovoltaic market, CZ silicon manufacture is under pressure to continuously lower costs and improve the cell efficiency. One way to accomplish this is to precisely control the melt/crystal interface and oxygen concentration during the growth process, because they are known to significantly influence the crystal quality, such as point defects, striations and light-induced degradation in solar cells [1,2].

Many studies have been performed to analyze the influence of the growth parameters on the melt/crystal interface shape [3–6] and oxygen concentration along the melt/crystal interface [7–10] during the CZ growth process by numerical simulations. It has been found that the maximum deflection of the melt/crystal interface decreases with faster crucible rotation [3–5], while deflection of the melt/crystal interface first decreases and then increases with increasing crystal rotation rate [3–6]. The crystal rotation rate has been identified as an important parameter for improving the consistency of the melt/crystal interface shape and reducing the temperature gradient along the interface. However, the oxygen concentration is likely to increase and the uniformity of the radial oxygen distribution at the interface gradually decreases with increasing crystal rotation rate [7,8]. Chen et al. [9,11] reported that it is possible to obtain a minimum oxygen concentration along the melt/crystal interface because the oxygen concentration first decreases and then increases with increasing crucible rotation rate. Because the heat and mass transfer in the crucible can significantly change for different combinations of crystal and crucible rotation rates, it may be possible to find the optimal combination of the crucible and crystal rotation rates to obtain the minimum deflection of the melt/crystal interface and oxygen concentration along the interface. However, these growth parameters interact with each other and their comprehensive effect cannot be estimated by qualitative deduction, and

* Corresponding authors.
E-mail addresses: wenchengma@ujs.edu.cn (W. Ma), ljliu@mail.xjtu.edu.cn (L. Liu).

https://doi.org/10.1016/j.jcrysgro.2020.125828
Received 8 July 2020; Received in revised form 2 August 2020; Accepted 4 August 2020
Available online 06 August 2020

an effective method to accurately control the melt/crystal interface shape and oxygen concentration along the interface at the same time is lacking.

Fühner et al. [12] combined a genetic algorithm (GA) with a heat transfer model to optimize the heat shield configuration with the aim of decreasing the deflection of the interface. However, they ignored the fluid flow because the global thermal simulation is very time consuming and the amount of data required by the optimization algorithm is not affordable. As a replacement for the time-consuming global simulation, some researchers have attempted to use an artificial neural network (ANN) model to rapidly evaluate the optimal crystal growth conditions [13–15]. Specifically, combination of a GA and an ANN is a promising and feasible approach for solving highly non-linear and non-local optimization problems, and it has been introduced into the crystal growth field to obtain the optimal growth conditions [16,17]. Asadian et al. [16] and Dang et al. [17] applied the optimization system of a GA and an ANN to the CZ YAG crystal and quasi-single crystalline silicon growth processes. It has been found that the efficiency of GA optimization can be improved by combining with an ANN, and several design parameters of the crystal growth system can be simultaneously optimized. The high diversity of the population is maintained to obtain global optimization solution. However, application of this optimization system to the CZ silicon growth process has not been reported. In this study, a two-dimensional (2D) global heat and mass transfer model was first used to simulate the CZ silicon crystal growth. The developed model was verified by experimental data and then used to design and train an ANN. An optimization system combining a GA with the ANN was used to optimize the growth parameters, including the crystal rotation rate and crucible rotation rate, with the aim of decreasing the deflection of the melt/crystal interface and oxygen concentration along the interface. Finally, the optimized variables were used in the heat and mass transfer model to evaluate the performance of the optimization system.

2. Models and methodology

2.1. Heat and mass transfer model

A schematic diagram of the industrial CZ furnace considered in this study is shown in Fig. 1. The heating in the furnace is resistance. The susceptor is made of graphite, which is used to hold the silica crucible during the growth process. The graphite resistance heater and graphite susceptor, as shown in Fig. 1, were widely used in the industrial Cz-Si furnace [18–20]. The diameters of the crucible and crystal are about 710 mm (28 in.) and 215 mm, respectively. The initial charge weight of silicon raw material is 390 kg. To increase the pulling rate, a conical shaped active crystal cooler with a water cooling system is installed around the crystal to enhance crystallization latent heat removal through the crystal.

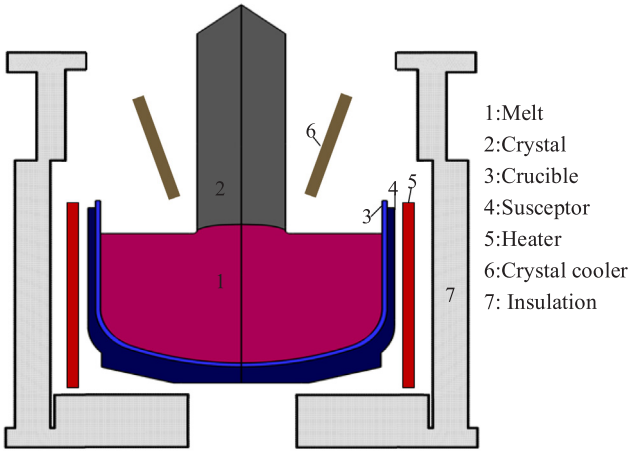

Fig. 1. Schematic diagram of the major components of the CZ furnace.

A global heat and mass transfer model was developed for the CZ silicon crystal growth process, taking into account melt convection, argon flow, conduction, thermal radiation, phase change and oxygen transport. In-house software (CGeMoS) for modeling and simulation of crystal growth/epitaxy, which is based on the finite volume method, was applied in this study. This software was developed and has been successfully used in our research for more than 10 years (see http://cgsolar.xjtu.edu.cn/) [20–22]. The near-wall grid is refined for better solution of heat and mass transfer in the furnace. In the present simulation, the total grid number was 67,800 and grid independence was validated. The major assumptions of the model are as follows [20]: (1) the furnace is considered to be 2D axisymmetric and the quasi-steady growth process is assumed, (2) all of the radiative surfaces are diffuse gray, (3) the silicon melt is assumed to be a Newtonian fluid, and (4) the ideal gas law is applied to argon gas. The argon and melt flows are turbulent and the standard k–ε model is adopted. With these assumptions, the governing equations of heat transfer for the silicon melt are given as follows:

$$\nabla\cdot\vec{u} = 0 \tag{1}$$

$$\nabla\cdot(\rho\vec{u}\vec{u}) = -\nabla p + \nabla\cdot[\mu_{eff}(\nabla\vec{u} + \nabla\vec{u}^{T})] - \rho\vec{g}\beta_{T}(T - T_{ref}) \tag{2}$$

$$\nabla\cdot(\rho C_{p}\vec{u}T) = \nabla\cdot(\lambda_{eff}\nabla T) \tag{3}$$

For other solid componets:

$$\nabla\cdot(\lambda\nabla T) + S_{Q} = 0 \tag{4}$$

where $\vec{u}$ is the velocity, ρ is the density, μ_{eff} is the effective dynamic viscosity, p is the pressure, T is the temperature, T_{ref} is the reference temperature, β_T is the thermal expansion coefficient, $\vec{g}$ is the gravity acceleration vector, C_p is the heat capacity, λ_{eff} is the effective thermal conductivity, S_Q is the heat generation rate per unit volume (equals zero for all solid components except the heater).

At the melt/crystal interface, the latent heat released and the heat flux satisfies the following equation:

$$\rho\Delta H V_{g} + \left(\lambda\frac{\partial T}{\partial n}\right)_{m} = \left(\lambda\frac{\partial T}{\partial n}\right)_{c} \tag{5}$$

where ΔH is the latent heat of crystallization, V_g is the crystal pulling rate, the subscript m and c denote the melt and crystal.

Along the melt-gas surface, both the gas shear stress and Marangoni tension were considered. Temperature continuity and heat flux conservation are kept at all interior boundaries between any two neighboring sub-domains. The temperature of the chamber wall is 300 K. The furnace pressure is kept at 13 Torr with an argon gas flow rate of 70 slpm. The pulling rate is 1.7 mm/min.

The governing equation for oxygen transport in the silicon melt is written as follows:

$$\nabla\cdot(\rho_{m}\omega_{O}\vec{u}_{m}) = \nabla\cdot\left[\left(\rho_{m}D_{O} + \frac{\mu_{t}}{Sc_{t}}\right)\nabla\omega_{O}\right] \tag{6}$$

The governing equation for SiO tranport in the argon gas is given as follows:

$$\nabla\cdot(\rho_{g}\omega_{SiO}\vec{u}_{g}) = \nabla\cdot\left[\left(\rho_{g}D_{SiO} + \frac{\mu_{t}}{Sc_{t}}\right)\nabla\omega_{SiO}\right] \tag{7}$$

where ω is the mass fraction, D is the molecular diffusivity, μ_t is the turbulent viscosity, Sc_t is the turbulent Schmidt number. The index symbols m, g, O and SiO denote the melt, gas, oxygen and SiO, respectively. The CO transport in the argon gas has the same expression form as that for SiO. The chemical equations corresponding to the generally accepted pathway for the oxygen transport are expressed in the following forms [23,24].

1. On the inside wall of the quartz crucible: $SiO_2(s) \leftrightarrow Si(m) + 2O(m)$
2. At the melt-gas interface (for O): $Si(\mathrm{m}) + O(m) \leftrightarrow SiO(g)$
3. At the graphite fixtures surfaces: $SiO(g) + 2C(s) \leftrightarrow CO(g) + SiC(s)$
4. Crucible/susceptor contact: $2SiO_2(s) + SiC(s) \leftrightarrow CO(g) + 3SiO(g)$
5. At the melt-gas interface (for C): $CO(g) \leftrightarrow C(m) + O(m)$
6. At the melt/crystal interface: $O(m) \leftrightarrow O(c)$

In the above reactions (1)-(6), the index symbols (s), (m), (g) and (c) denote solid, melt, gas and crystal, respectively. The corresponding boundary conditions for the impurity species transport in the silicon and argon gas regions are defined as follows:

(a) On the inside wall of the quartz crucible, reaction (1) occurs and the equilibrium concentration of O is expressed as follows [25]:

$$c_O = 0.5 \times 10^{23} \times \frac{exp(-3200/T - 8.19)}{1 - exp(-3200/T - 8.19)} \tag{8}$$

(b) At the melt-gas interface, O, C, SiO and CO coexist. Reactions (2) and (5) describe O and C transport, respectively. Equilibrium relationships for the same element between the silicon melt and argon gas are given as follows [26]:

$$c_{\mathrm{SiO}} = \frac{101325}{RT}\frac{c_{\mathrm{O}}}{c_{\mathrm{Si}}}e^{-21000/T+17.8} \tag{9}$$

$$c_{\mathrm{CO}} = \frac{101325}{RT}\frac{c_{\mathrm{O}}}{c_{\mathrm{Si}}}\frac{c_{\mathrm{C}}}{c_{\mathrm{Si}}}e^{-5210/T+14.6} \tag{10}$$

where c_{SiO} and c_{CO} are the molar concentrations of SiO and CO in the argon gas, respectively, c_{O} and c_{C} are the molar concentrations of O and C in the silicon melt, repectively, and R is the universal gas constant, which is equal to 8.314 J/mol·K.

Two more boundary conditions are needed to solve the four unknown variables at the melt-gas surface according to the law of mass conservation:

$$c_{Ar}\left(D_{SiO} + \frac{\mu_t}{\rho_{Ar}Sc_t}\right)\nabla\left(\frac{c_{SiO}}{c_{Ar}}\right) + c_{Ar}\left(D_{CO} + \frac{\mu_t}{\rho_{Ar}Sc_t}\right)\nabla\left(\frac{c_{CO}}{c_{Ar}}\right) = c_{Si}\left(D_O + \frac{\mu_t}{\rho_{Si}Sc_t}\right)\nabla\left(\frac{c_O}{c_{Si}}\right) \tag{11}$$

$$c_{Ar}\left(D_{CO} + \frac{\mu_t}{\rho_{Ar}Sc_t}\right)\nabla\left(\frac{c_{CO}}{c_{Ar}}\right) = c_{Si}\left(D_O + \frac{\mu_t}{\rho_{Si}Sc_t}\right)\nabla\left(\frac{c_O}{c_{Si}}\right) \tag{12}$$

(c) The SiO reacts with carbon at the surfaces of the hot graphite fixtures to generate CO. Reaction (3) is assumed to be reversible and the Gibbs free energy of the reaction is expressed as follows [26]:

$$\begin{aligned}\Delta G &= -81300 + 3.02T \text{ J/mol, T} < 1640\text{K}\\ \Delta G &= -22100 - 33.1T \text{ J/mol,1640K} < \text{T} < 1687\text{K}\\ \Delta G &= -72100 - 3.44T \text{ J/mol, T} > 1687\text{K}\end{aligned} \tag{13}$$

The equilibrium constant of the reaction is $\mathrm{K} = \mathrm{e}^{-\Delta G/RT}$. The coupled boundary conditions at the graphite fixtures' surfaces can be expressed as:

$$c_{\mathrm{Ar}}\left(D_{\mathrm{SiO}} + \frac{\mu_t}{\rho_{\mathrm{Ar}}Sc_t}\right)\nabla\left(\frac{c_{\mathrm{SiO}}}{c_{\mathrm{Ar}}}\right) = -c_{\mathrm{Ar}}\left(D_{\mathrm{CO}} + \frac{\mu_t}{\rho_{\mathrm{Ar}}Sc_t}\right)\nabla\left(\frac{c_{\mathrm{CO}}}{c_{\mathrm{Ar}}}\right) \tag{14}$$

$$c_{\mathrm{CO}}/c_{\mathrm{SiO}} = K \tag{15}$$

where D_{SiO} and D_{CO} are the molecular diffusivities of SiO and CO in the argon gas, respectively, which can be expressed as:

$$D_{\mathrm{SiO}} = 8.62611 \times 10^{-6}T^{1.75}/p \tag{16}$$

$$D_{\mathrm{CO}} = 1.79548 \times 10^{-5}T^{1.75}/p \tag{17}$$

(d) When the temperature of the quartz exceeds approximately 1200 K, the quartz begins to soften and deform. Reactions (3) and (4) are sequentially involved the contact reaction between quartz crucible and graphite susceptor. The Gibbs free energy for generating SiO and CO in reaction (4) was computed and found to be as follows:

$$\Delta G = 1444316.8 - 682.0T \text{ J/mol} \tag{18}$$

$$K = \frac{a_{SiO(g)}^3 a_{CO(g)}}{a_{SiC(s)}a_{SiO_2(s)}^2} = e^{-\Delta G/RT} \tag{19}$$

where the activities of the species a are expressed as follows:

$$\begin{aligned}a_{SiO_2(s)} &= 1,\ a_{SiC(s)} = c_{SiC(s)}/c_{SiO_2(s)}\\ a_{SiO(g)} &= 154885e^{-43430/T+20.5}/101325\\ a_{CO(g)} &= 51628e^{-43430/T+20.5}/101325\end{aligned} \tag{20}$$

(e) At the crystallization front, oxygen are segregated into the crystal and the law of mass conservation is expressed as [27]:

$$\left(D_O + \frac{\mu_t}{\rho_{Si}Sc_t}\right)\frac{\partial c_O}{\partial n} + V_g c_O(1 - k_{seg}) = 0 \tag{21}$$

where k_{seg} is the segregation coefficients of oxygen.

The relationship between the mass fraction ω and the molar concentration c in the aforementioned equations and boundary conditions is $c = \rho\omega/M$, where M is the atomic weight of the impurity species. The major thermophysical properties of the components in the CZ furnace are shown in Table 1 and Table 2 [28].

2.2. ANN

The ANN method is a mathematical method used for estimation of unknown functions, especially for approximation of unknown nonlinear functions [13]. An ANN is characterized by a set of artificial neurons and the connections between them. Each neuron receives inputs and processes them before giving the final outputs. The typical structure of an ANN consists of three layers, including input, hidden and output layers. An ANN receives inputs by neurons in the input layer (first layer) and its output is returned by the neurons in the output layer (final layer). The neuron number of the input layer of the ANN is determined by the number of variables selected, and the neuron number

Table 1
Thermal properties of components in the CZ furnace.

Components	Density(kg/m^3)	Heat capacity(J/(kg·K))	Thermal conductivity W/(m·K)	Emissivity factor —
Silicon melt	2530	1000	64	0.3
Silicon crystal	2330	1059	22	0.3
Graphite	2300	2019	90	0.8
Quartz crucible	2650	1232	4	0.85
Furnace wall	7900	477	15	0.6
Argon gas	–	520.64	$0.01 + 2.5 \times 10^{-5}T$	–
Insulation	2101	$-317 + 4.03T - 2.4 \times 10^{-4}T^2 + 5.0 \times 10^{-7}T^3$	$0.334 - 1.83 \times 10^{-4}T + 2.15 \times 10^{-7}T^2 - 1.89 \times 10^{-11}T^3 - 2.08 \times 10^{-11}T^3$	0.45

Table 2
Thermal properties of fluids in the system.

Fluids	Latent heat (J/kg)	Thermal expansion coefficient (K^{-1})	Dynamic viscosity (kg/(m·s))	Melting temperature (K)
Melt	1,411,000	1.4×10^{-4}	7.0×10^{-4}	1685
Argon	–	–	$8.466 \times 10^{-6} + 5.365 \times 10^{-8}T – 8.68 \times 10^{-12}T^2$	–

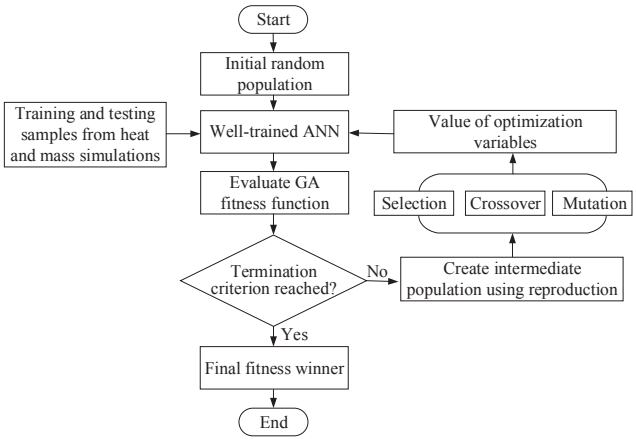

Fig. 2. Optimization process using GA and ANN models.

of the output layer is determined by the number of objective indexes. There may be one or more intermediate layers, which are called hidden layers. The most common output operations for the j-th neurons in the hidden or output layers are as follows:

$$O_j = A\left(\sum_{i=1}^{n} w_{ji} \cdot x_i + b_j\right) \tag{22}$$

where w_{ji} is the weight of the connection from the i-th neuron of the preceding layer to the j-th neuron of the considered layer, x_i is the input value for each neuron, and b_j and A are the bias and activation function, respectively. The weights of the connections and biases of the artificial neurons are adjusted by the quantities of sets of inputs and outputs to obtain the targeted output for a specific combination of inputs. The goal of network training is to adjust the w_{ji} and b_j values of specific neurons to minimize the error and accurately reflect the relationship between the inputs and outputs. The precision of an ANN model largely depends on the diversity and reservoir of the training data, which are obtained either from numerical simulations or experiments. Owing to the high cost of experiments, the global heat and mass transfer model was applied to generate the training and testing data for designing the ANN model.

2.3. GA

As a class of parallel iterative searching algorithms, GAs can be regarded as self-adaptive sampling techniques or black box search routines. In a GA, sets of variables are coded and represented by bit strings of fixed length, which are known as chromosomes. The chromosomes in the evolution process of a GA usually experience selection, crossover and mutation after initialization until the convergence condition is satisfied. Starting with random initialization, the selection operator can select a "good" solution as seeds. The roulette wheel selection scheme is used in this study. In the selection procedure, individuals with better fitness values have more chance of being selected to participate in the next generation. The selection probability of each individual X_i is

$$P_s(X_i) = \frac{f(X_i)}{\sum_{i=1}^{n} f(X_i)},\ \mathrm{i} = 1,2,\cdots,\mathrm{n} \tag{23}$$

where n is the number of individuals in the population and $f(X_i)$ is a fitness value.

The single-point crossover method is used to generate a new individual with crossover probability P_c, which hopefully inherits the good features from the parents. Two parents X and Y are randomly selected after the selection operation. One point is then randomly chosen to separate the chromosome of parents X and Y, and children X' and Y' are obtained as offspring as follows:

$$\begin{cases} X' = \xi X + (1-\xi)Y \\ Y' = \xi Y + (1-\xi)X \end{cases} \tag{24}$$

where ξ is a random number in the range 0–1.

The mutation operator is performed to avoid local optima in the search space and maintain some level of diversity. The new individuals X' and Y' will mutate with mutation probability P_m by randomly changing the individual in the bit string. In this study, we used a non-uniform mutation operator, which is dynamically reduced with increasing number of generations to accelerate convergence in the early generations and avoid premature convergence in the late generations [17].

2.4. Optimization system combination with an ANN and a GA

The operation flow of the global heat and mass transfer model combined with the ANN and GA optimization system is demonstrated in Fig. 2. The global heat and mass transfer model was applied to generate training data for the ANN. As mentioned in our previous work [17], the random searching algorithm of the GA in the optimization procedure requires huge numbers of input and output parameters. It would be immeasurable in terms of computational resource and time to perform traditional heat and mass simulations to feed the GA optimization process. Therefore, as a replacement of the global heat and mass simulations in the optimization system, a well-trained ANN model acted as a rapid response database. In this study, the initial populations were the crucible rotation rate (Ω_c) and crystal rotation rate (Ω_s). The objective functions consisted of two parts: the deflection of melt/crystal interface and the average oxygen concentration along the melt/crystal interface. In the first step, an initial population is created by randomly placing 1 s and 0 s into the populations' bit strings. All of the random populations are evaluated according to the objective or fitness function based on the ANN. Generally, objective functions are directly taken as the fitness function or some proper transformations are performed. During the optimization process, genetic operations, such as selection, crossover and mutation procedures, are applied to reproduce a new generation. This process is repeated until the termination criterion has been reached. In general, this criterion is defined as a certain number of iterations or a satisfactory objective value. Finally, pairs of individuals win according to their fitness values. The validity of the optimal results from the optimization system is confirmed by using the heat and mass transfer model or experimental data.

3. Results and discussion

3.1. Preliminary analysis

The global heat and mass transfer model was first verified by available experimental data. In the experiment, the original crystal and

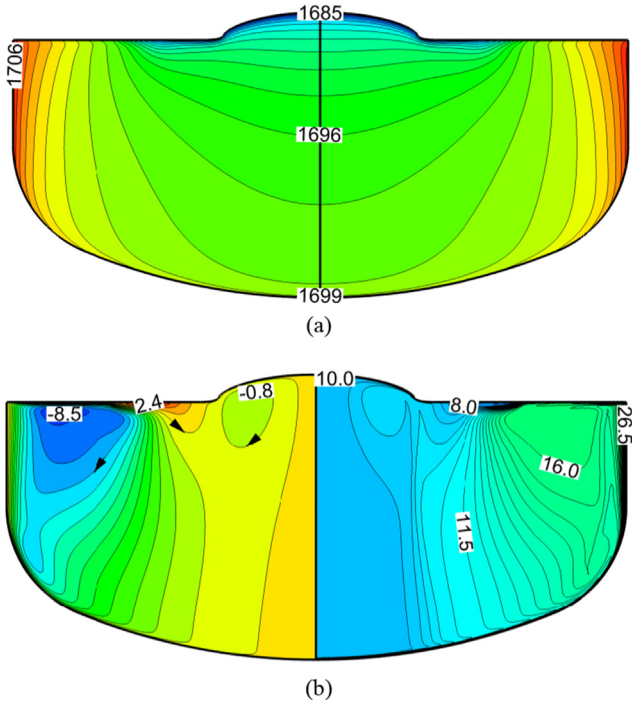

Fig. 3. Distributions of the temperature and oxygen concentration in the melt at the crystal length of 2000 mm: (a) temperature (ΔT = 1 K) and (b) stream function (left, unit: 10^{-2} kg/s) and oxygen concentration (right, ΔCo = 0.5 ppma).

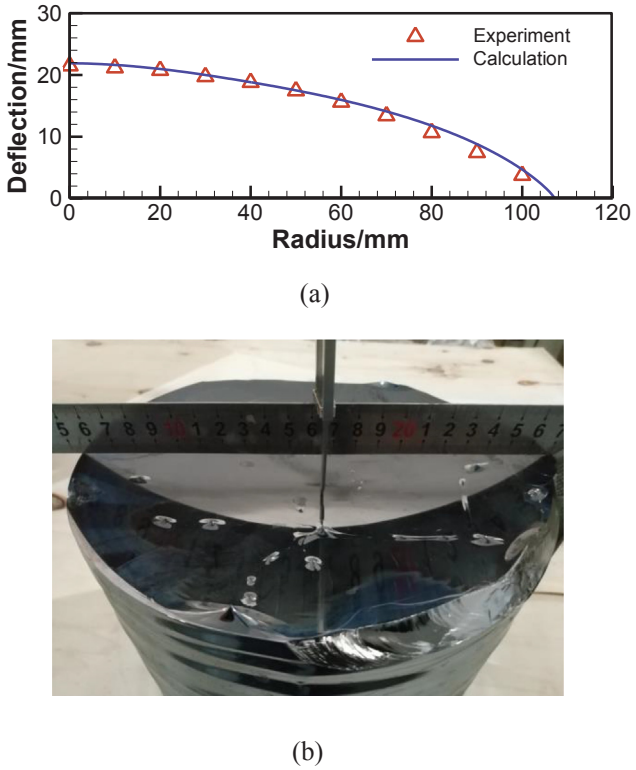

Fig. 4. Deflection of the melt/crystal interface: (a) comparison between experiment and calculation and (b) measurement by the quick pulling separation method.

crucible rotation rates were 9 and −8 rpm, respectively. The negative rotation rate indicates counter rotation of the crucible and crystal. A numerical simulation was performed under the same growth conditions as the experiment. The distributions of the temperature and streamlines, as well as the oxygen concentration in the silicon melt at the crystal length of 2000 mm are shown in Fig. 3. The maximum temperature was located at the vertical wall of the silicon melt, because the graphite heater was located around the crucible and directly radiated heat on the side wall of the crucible. The temperature at the bottom was relatively low. From the right part of Fig. 3(b), three main vortices existed in the melt: a Taylor-Proudman vortex beneath the crystal, a large buoyancy vortex near the crucible wall and a small thermocapillary vortex between them. The Taylor-Proudman vortex formed because of the forced convection generated by the crystal and crucible rotation. It is clear that the flow pattern in the melt significantly influenced the heat and mass transfer, and it also affected the distributions of the interface shape and oxygen concentration. The maximal oxygen concentration occurred at the location of the maximum temperature at the crucible wall. Larger oxygen concentration gradients occurred in the regions near the crucible wall and the melt surface owing to oxygen dissolution and evaporation, respectively [8]. In the experiments, crystals with a diameter of 215 mm were grown in the industrial CZ furnace. Three wafers were cut from three different crystals at the same position, i.e. at the same crystal length of 2000 mm. The interstitial oxygen concentrations at the central point of these wafers were measured by FTIR spectrometry. The measured average value of the oxygen concentrations was about 10.20 ppma (5.66×10^{17} atoms/cm^3). The calculated value of the oxygen concentration at the central point of the melt/crystal interface at the crystal length of 2000 mm was 9.91 ppma (5.50×10^{17} atoms/cm^3), corresponding to a concentration of 9.89 ppma (5.49×10^{17} atoms/cm^3) in the crystal because the segregation coefficient of oxygen is 0.998 in the simulation [19]. Therefore, the calculated oxygen concentration is in good agreement with the experimental data. A comparison of the melt/crystal interface shape between the simulation and experiment is shown in Fig. 4(a). The interface was concave to the crystal (observed from the crystal side). The experimental melt/crystal interface shape was acquired by the quick pulling separation method, as shown in Fig. 4(b). The simulation results and experimental data agree reasonably well. Therefore, the global heat and mass transfer model was validated. This model was then used to simulate the CZ silicon crystal growth process under different combinations of crystal and crucible rotation rates.

Table 3
Mean square error (MSE) of ANN with one hidden layer and 2–10 neurons from 10-fold cross validation.

Hidden neurons	2	3	4	5	6	7	8	9	10
Average MSE/10^{-3}	57	21	15	20	18	16	23	38	27

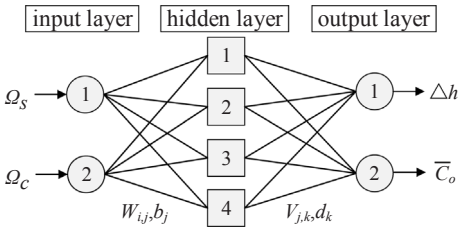

Fig. 5. Resulting architecture of the ANN with two inputs, two outputs and one hidden layer with four neurons. The arrows and lines represent the information flow.

3.2. ANN training

The ANN was designed to quickly map the complex non-linear relationships between the optimization variables and targets. The key target of the interface deflection Δh is defined as the height difference

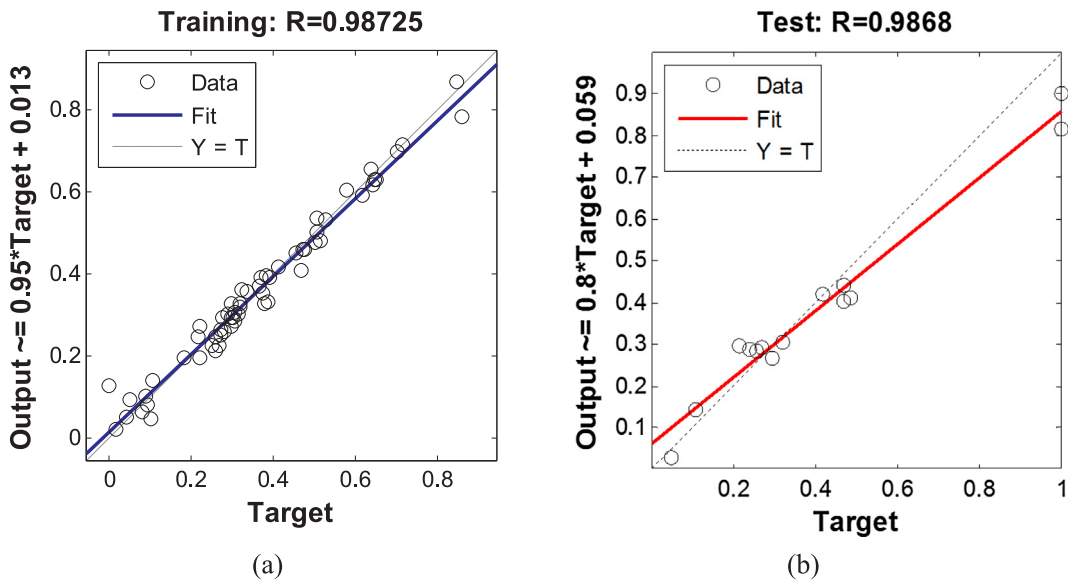

Fig. 6. The correlation coefficients between simulation results of 2D global model (target) and ANN predicted responses (output): (a) training cases and (b) test cases.

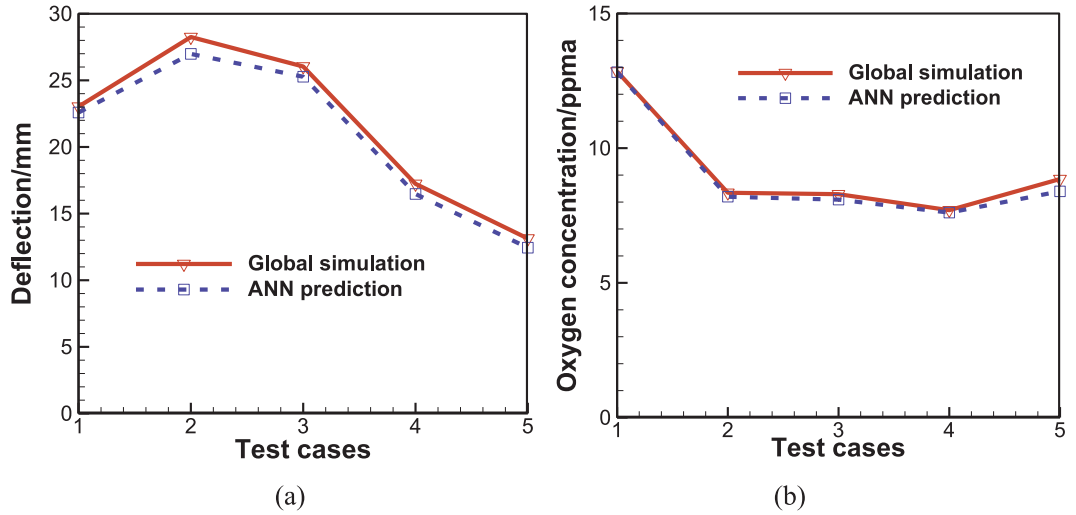

Fig. 7. Comparison between calculation and ANN prediction: (a) deflection of the melt/crystal interface and (b) average oxygen concentration along the interface.

Table 4
Parameters of the GA.

String length	Crossover probability	Mutation probability	Generations	Individuals
25	0.7	non-uniform mutation	100	30

between the centre point of the interface and the triple point. The key target of the oxygen concentration is represented by the average oxygen concentration along the melt/crystal interface. As previously discussed, the ultimate success of an ANN depends on the availability of numerous and diverse data sets. A series of numerical simulations for different combinations of crystal and crucible rotation rates was performed to generate training samples for the ANN. The ranges of the crystal and crucible rotation rates were 0 to 32 and −18 to 0, respectively. The values of the two key targets were extracted from the simulation results based on the verified global heat and mass transfer model. Eventually, 50 sets of inputs and outputs were selected for the ANN. Levenberg–Marquardt back propagation was used as the training algorithm. The sigmoidal and pureline activation function was applied

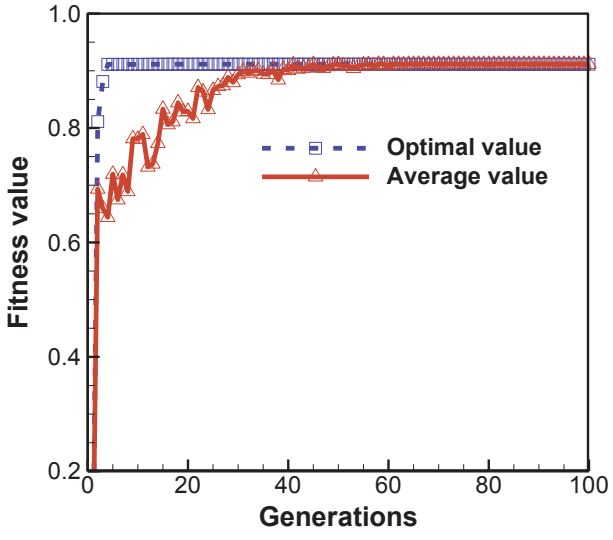

Fig. 8. Evolution of the best and average fitness values during GA optimization.

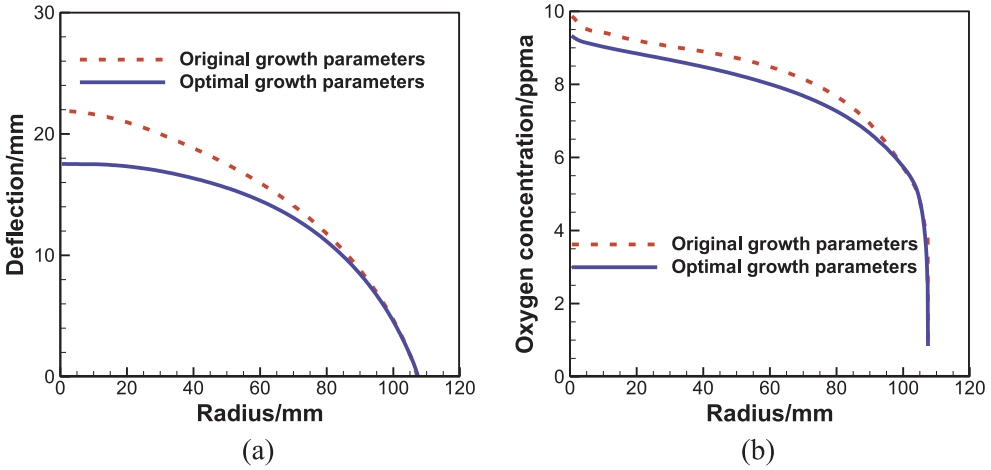

Fig. 9. Comparison of the original and optimal cases: (a) melt/crystal interface shape and (b) oxygen concentration along the interface.

between the input layer and hidden layer, as well as between the hidden layer and output layer. 10-fold cross-validation was performed for structured networks with different hidden layer neuron numbers in the range 2–10 neurons [29]. The results are given in Table 3. The ANN reached the lowest mean square error (MSE) when the hidden layer had 4 neurons and therefore this number of neurons was selected for further calculation. A three-layer ANN model with one hidden layer and 4 neurons was thus constructed, as shown in Fig. 5. The correlation coefficients between simulation results from 2D global heat and mass transfer model and ANN predicted responses are given in Fig. 6. The correlation coefficient corresponding to the best linear regression of ANN outputs to targets reached 0.98725 for the training cases and 0.9868 for the test cases.

Fig. 7 compares the melt/crystal interface deflection and average oxygen concentration along the interface between calculation and ANN prediction. The highest relative errors between the numerical results and predicted values of the ANN for the interface deflection and average oxygen concentration for the test cases were 5.27% and 5.19%, respectively, which are satisfactory. This well-trained ANN model was used to quickly evaluate the fitness value in the GA, with the advantages of saving computing time and resource compared with traditional global heat and mass transfer computations.

3.3. Optimization results from the GA

In this study, a two-objective optimization problem was considered. The design parameters were the crystal and crucible rotation rates. The optimization algorithm was performed based on the combined ANN and GA model. A flat melt/crystal interface shape and a low oxygen concentration are necessary to ensure the high quality of the CZ silicon crystal [2,19]. The objective of optimization is to reduce melt/crystal interface deflection and the oxygen concentration along the interface. Therefore, the objective functions can be expressed as:

Minimize

$$f(\omega_s, \omega_c) = w_1 |\Delta h| + w_2 |\bar{C}_o| \tag{25}$$

Subject to

$$\begin{aligned} &0 \leqslant \Omega_s \leqslant 32 \text{ rpm} \\ &-18 \leqslant \Omega_c \leqslant 0 \text{ rpm} \end{aligned} \tag{26}$$

where w_1 and w_2 are the weighting factors. To enhance the search efficiency of the GA and improve the local search ability, we performed an exponential transformation of the objective functions to construct the fitness function. By doing this, the fitness values of interface deflection and average oxygen concentration are limited to the range of 0–1. In this research, w_1 and w_2 are taken to be 0.5 according the discussion with our industrial partners. The parameters of the GA used for the calculations are given in Table 4.

The best and average fitness values with the evolution process during GA optimization are shown in Fig. 8. At the beginning, each individual was scattered all over the space, and it gradually converged along with evolution. Although the best fitness and average fitness developed in different ways with different generations, all of the 30 individuals converged to one point at the 78th generation. The optimal crystal and crucible rotation rates obtained from the ANN and GA optimization system were 11.06 and −13.78 rpm, respectively.

3.4. Evaluation of the optimization results

To evaluate the performance of the optimization model, the optimal growth parameters were applied in the global heat and mass model to predict the melt/crystal interface shape and oxygen concentration. A comparison of the melt/crystal interface shapes for the original and optimal parameters is shown in Fig. 9(a). The maximum deflection of the interface was only 17.53 mm in the optimal case, which represents a reduction of 19.92% compared with the original parameters (deflection of 21.89 mm). The oxygen concentration distributions for the original and optimal cases are shown in Fig. 9(b). The oxygen concentration along the melt/crystal interface decreased from the centre of the melt/crystal interface to the crystal edge in both cases. The oxygen concentration in the optimal case was lower than that obtained with the original parameters, especially in the central part, leading to higher radial uniformity of the oxygen concentration. Compared with the original case, the average oxygen concentration in the optimal case was 7.34 ppma (4.07×10^{17} atoms/cm^3) with a decrease of about 4.43%. Therefore, the two key targets in the optimal case were superior to those in the original case. This indicates that the optimization system can obtain the optimal results, which cannot be easily achieved by qualitative improvement through theoretical analysis.

4. Conclusions

A 2D global heat and mass transfer model has been developed to simulate the CZ monocrystalline silicon crystal growth process and validated by experimental measurements. The ANN prediction model was trained using output indicators of the crystal quality from the validated heat and mass transfer model. The results showed that the constructed ANN model can well predict the results of global heat and mass transfer simulations of the CZ silicon crystal growth process. The optimization system combining a GA with a well-trained ANN model was used to optimize the growth parameters (the rotation rates of the crystal and crucible) to achieve a flatter melt/crystal interface and

lower oxygen concentration along the interface. Optimized values of 11.06 and −13.78 rpm were obtained for the crystal and crucible rotation rates, respectively. The optimized melt/crystal interface deflection and oxygen concentration along the interface obtained by the optimization system were finally compared with those obtained from the heat and mass transfer model using the optimal growth parameters, and they agreed reasonably well. Compared with the original growth parameters, the deflection of the interface and average oxygen concentration along the interface were reduced by about 19.92% and 4.43%, respectively.

CRediT authorship contribution statement

Xiaofang Qi: Conceptualization, Methodology, Data curation, Writing - original draft, Writing - review & editing. **Wencheng Ma:** Methodology, Software, Data curation, Writing - original draft. **Yifan Dang:** Formal analysis, Methodology, Software. **Wenjia Su:** Visualization, Investigation. **Lijun Liu:** Supervision, Writing - review & editing.

Declaration of Competing Interest

There are no conflicts to declare.

Acknowledgements

This research was supported by the Key Research and Development Program of Jiangsu Province, China (Grant No. BE2019009-003), the China Postdoctoral Science Foundation, China (Grant No. 2019M651731), the National Natural Science Foundation of China, China (Grant No. 51906086) and Jiangsu Post-doctoral Research Support Program, China (Grant No. 2018K100C).

References

[1] P. Rudolph, Handbook of Crystal Growth, Elsevier, 2015.
[2] J.L. Ding, L.J. Liu, Real-time prediction of crystal/melt interface shape during Czochralski crystal growth, CrystEngComm 20 (2018) 6925–6931.
[3] N. Kobayashi, T. Arizumi, The numerical analyses of the solid-liquid interface shapes during the crystal growth by the Czochralski method. Part II. effects of the crucible rotation, Jpn. J. Appl. Phys. 9 (1970) 1255–1259.
[4] O.A. Noghabi, M. M'Hamdi, M. Jomâa, Effect of crystal and crucible rotations on the interface shape of Czochralski grown silicon single crystals, J. Cryst. Growth 318 (2011) 173–177.
[5] R. Teng, Q. Chang, Y. Li, B. Cui, Q.H. Xiao, G.H. Zhang, Numerical analysis of solid–liquid interface shape during large-size single crystalline silicon with Czochralski method, Rare Met. 36 (2017) 289–294.
[6] O.A. Noghabi, M. Jomâa, M. M'Hamdi, Analysis of W-shape melt/crystal interface formation in Czochralski silicon crystal growth, J. Cryst. Growth 362 (2013) 77–82.
[7] J. Zhang, J.C. Ren, D. Liu, Effect of crucible rotation and crystal rotation on the oxygen distribution at the solid-liquid interface during the growth of Czochralski monocrystalline silicon under superconducting horizontal magnetic field, Results Phys. 13 (2019) 102127.
[8] T.H.T. Nguyen, J.C. Chen, C. Hu, C.H. Chen, Numerical simulation of heat and mass transfer during Czochralski silicon crystal growth under the application of crystal-crucible counter- and iso-rotations, J. Cryst. Growth 507 (2019) 50–57.
[9] J.C. Chen, Y.Y. Teng, W.T. Wun, C.W. Lu, H.I. Chen, C.Y. Chen, W.C. Lan, Numerical simulation of oxygen transport during the CZ silicon crystal growth process, J. Cryst. Growth 318 (2011) 318–323.
[10] X. Liu, H. Harada, Y. Miyamura, X.F. Han, S. Nakano, S.I. Nishizawa, K. Kakimoto, Transient global modeling for the pulling process of Czochralski silicon crystal growth. II. Investigation on segregation of oxygen and carbon, J. Cryst. Growth 532 (2020) 125404.
[11] J.C. Chen, P.C. Guo, C.H. Chang, Y.Y. Teng, C. Hsu, H.M. Wang, C.C. Liu, Numerical simulation of oxygen transport during the Czochralski silicon crystal growth with a cusp magnetic field, J. Cryst. Growth 401 (2014) 888–894.
[12] T. Fühner, T. Jung, Use of genetic algorithms for the development and optimization of crystal growth processes, J. Cryst. Growth 266 (2004) 229–238.
[13] N. Dropka, M. Holena, Optimization of magnetically driven directional solidification of silicon using artificial neural networks and Gaussian process models, J. Cryst. Growth 471 (2017) 53–61.
[14] Z.J. Chen, W.H. Ma, K.X. Wei, J.J. Wu, S.Y. Li, K.Q. Xie, G.Q. Lv, Artificial neural network modeling for evaluating the power consumption of silicon production in submerged arc furnaces, Appl. Therm. Eng. 112 (2017) 226–236.
[15] Y. Tsunooka, N. Kokubo, G. Hatasa, S. Harada, M. Tagawa, T. Ujihara, High-speed prediction of computational fluid dynamics simulation in crystal growth, CrystEngComm 20 (2018) 6546–6550.
[16] M. Asadian, S.H. Seyedein, M.R. Aboutalebi, A. Maroosi, Optimization of the parameters affecting the shape and position of crystal–melt interface in YAG single crystal growth, J. Cryst. Growth 311 (2009) 342–348.
[17] Y.F. Dang, L.J. Liu, Z.Y. Li, Optimization of the controlling recipe in quasi-single crystalline silicon growth using artificial neural network and genetic algorithm, J. Cryst. Growth 522 (2019) 195–203.
[18] X. Liu, H. Harada, Y. Miyamura, X.F. Han, S. Nakano, S.I. Nishizawa, K. Kakimoto, Transient global modeling for the pulling process of Czochralski silicon crystal growth. I. Principles, formulation, and implementation of the model, J. Cryst. Growth 532 (2020) 125405.
[19] B. Zhou, W.L. Chen, Z.H. Li, R.C. Yue, G.W. Liu, X.M. Huang, Reduction of oxygen concentration by heater design during Czochralski Si growth, J. Cryst. Growth 483 (2018) 164–168.
[20] W.H. Zhao, L.J. Liu, Control of heat transfer in continuous-feeding Czochralski-silicon crystal growth with a water-cooled jacket, J. Cryst. Growth 458 (2017) 31–36.
[21] X.F. Qi, L.J. Liu, W.C. Ma, Effects of furnace pressure on oxygen and carbon coupled transport in an industrial directional solidification furnace for crystalline silicon ingots, J. Cryst. Growth 468 (2017) 933–938.
[22] L.J. Liu, Q.H. Yu, X.F. Qi, W.H. Zhao, G.X. Zhong, Controlling solidification front shape and thermal stress in growing quasi-single-crystal silicon ingots: Process design for seeded directional solidification, Appl. Therm. Eng. 91 (2015) 225–233.
[23] L.J. Liu, W.C. Ma, X.F. Qi, Z.Y. Li, Y.F. Zhang, Global simulation of coupled oxygen and carbon transport in an industrial directional solidification furnace for crystalline silicon ingots: Effect of crucible cover coating, Int. J. Heat Mass Transf. 108 (2017) 2355–2364.
[24] X. Liu, S. Nakano, K. Kakimoto, Development of carbon transport and modeling in Czochralski silicon crystal growth, Cryst. Res. Technol. 52 (2017) 1600221.
[25] K.W. Yi, K. Kakimoto, Z.G. Niu, M. Eguchi, H. Noguchi, S. Nakamura, K. Mukai, Asymmetric distribution of oxygen concentration in the si melt of a Czochralski system, J. Electrochem. Soc. 143 (1996) 722.
[26] D.E. Bornside, R.A. Brown, T. Fujiwara, H. Fujiwara, T. Kubo, The effects of Gas-phase convection on carbon contamination of Czochralski-grown silicon, J. Electrochem. Soc. 142 (1995) 2790.
[27] L.J. Liu, K. Kakimoto, T. Taishi, K. Hoshikawa, Computational study of formation mechanism of impurity distribution in a silicon crystal during solidification, J. Cryst. Growth 265 (2004) 399–409.
[28] J.L. Ding, L.J. Liu, W.H. Zhao, Enhancement of heat transfer in Czochralski growth of silicon crystals with a chemical cooling technique, J. Cryst. Growth 468 (2017) 894–898.
[29] R.R. Picard, R.D. Cook, Cross-validation of regression models, J. Am. Stat. Assoc. 79 (1984) 575–583.